Article ID: 1000-324X(2019)10-1128-05 **DOI:** 10.15541/jim20190005

Thermodynamic Stability and Thermal Expansion of Pure-phase $BiFeO_3$

CHENG Guo-Feng, RUAN Yin-Jie, SUN Yue, YIN Han-Di

(Analysis and Testing Center for Inorganic Materials, Shanghai Institute of Ceramics, Chinese Academy of Sciences, Shanghai 200050)

Abstract: The thermodynamic stability and thermal expansion of pure-phase $BiFeO_3$ multiferroic are studied using *in-situ* high temperature X-ray diffraction (HT-XRD), and high temperature Raman spectroscopy (HT-Raman). $BiFeO_3$ keeps its rhombohedral structure with space group of *R3c* in heating process. However, minor $BiFeO_3$ could decompose to $Bi_2Fe_4O_9$ and $Bi_{25}FeO_{39}$ in cooling process, which may be induced by its oxygen octahedron tilt distortion. In addition, the thermal expansion coefficients of $BiFeO_3$ are also investigated, showing an isotropic and positive behavior. These results are further confirmed by Raman spectrum analysis. This work may benefit for the preparation of pure-phase $BiFeO_3$.

Key words: $BiFeO_3$; phase transition; thermal expansion coefficients; HT-XRD; HT-Raman

Multiferroic materials couple ferromagnetic and ferroelectric properties simultaneously, in which $BiFeO_3$ (BFO) is one of the well-known single-phase materials[1-2]. It has a G-type antiferromagnetic and ferroelectric behavior with higher Néel temperature (T_N~370 ℃) and Curie temperature (T_C~810 ℃)[3]. It is reported to have a rhombohedrally distorted perovskite structure with *R3c* space group[4]. Recently, many attempts have been made to improve the ferroelectricity and magnetization in BFO, such as ion-doping, epitaxial films, single crystals and nanoparticles[5-7], it is very difficult to synthesize pure BFO ceramic for its narrow phase stabilized temperature range and low peritectic decomposition temperature[8-9]. In order to remove the Fe-rich ($Bi_2Fe_4O_9$) and Bi-rich ($Bi_{25}FeO_{39}$) phases, many efforts have been done such as rapid liquid phase sintering, quenching process, leaching with dilute nitric acid[10-13]. Although these methods are very effective, the thermodynamic stability and decomposition of $BiFeO_3$ are currently still not clarified. Selbach, *et al*[14] reported the decomposition of $BiFeO_3$ to $Bi_{25}FeO_{39}$ and $Bi_2Fe_4O_9$ in the temperature interval 447–767 ℃ for its metastable property. In our previous study, $BiFeO_3$, $Bi_{25}FeO_{39}$ and $Bi_2Fe_4O_9$ phases are not in thermodynamic stable status during the cooling sintering process[15]. In addition, many works focus on the thermal expansion and transformation of $BiFeO_3$ solid solutions. Chen, *et al*[16] reported the negative thermal expansion and unusual transformation in $PbTiO_3$- $BiFeO_3$. Bhattacharjee, *et al*[17] studied the associated giant negative thermal expansion for $(1–x)BiFeO_3–xPbTiO_3$ (x=0.31) solid solution system. Klyndyuk and Chen, *et al*[18-19] investigated the linear thermal expansion coefficient of $BiFeO_3$-$NdMnO_3$ and $(1–x)$ $BiFeO_3–xLaFeO_3$, respectively. Nevertheless, the clear pictures on thermal stability and thermal expansion characteristics for either BFO or doped BFO are very limited.

To address the issue, we synthesized pure BFO powder, studied its thermodynamic stability and thermal expansion by *in-situ* HT- XRD and HT-Raman. This work would provide a useful experimental guidance for the preparation of pure-phase BFO by clarifying its thermodynamic stability and thermal expansion characters.

1 Experimental

The BFO ceramic was prepared by a combined method of solid state reaction and quenching using Bi_2O_3 and Fe_2O_3. Minor $Bi_{25}FeO_{39}$ phase in the ceramic was leached by dilute nitric acid. The crystal structure of pure BFO powder was characterized by HT-XRD using Bruker D8 ADVANCE X-ray diffractometer with the heating rate 30 ℃·min^{-1} in air. Data were collected from 20° to 110° (2θ) in the step scanning mode (step size=0.02°, FT=1.5 s) in the temperature range of 25–800 ℃ and 700–25 ℃. The lattice parameters and unit-cell volumes were calculated by Rietveld refinements based on TOPAS software. This refinement modeled the background and peak shape by a fifth order polynomial and a Pseudo-

Received date: 2019-01-03; **Modified date:** 2019-03-27
Foundation item: National Natural Science Foundation of China (51202280); Shanghai Technical Platform for Testing and Characterization on Inorganic Materials (14DZ2292900)
Biography: CHENG Guo-Feng (1977–), male, senior engineer. E-mail: gfcheng@mail.sic.ac.cn

Voigt II function, respectively. Backscattered Electron (BSE) images and Energy-dispersive Spectrometry (EDS) quantitative measurement were carried out by a Scanning Electron Microscope (FEI MAGELLAN 400). The Raman spectra of pure BFO powder at the temperature range 25–750 ℃ were examined using a Renishaw confocal Raman spectroscopy (model inVia). The laser power was maintained at 0.2 mW with semiconductor laser excitation at 532 nm.

2 Results and discussion

The thermodynamic stability of pure BFO powder is performed by the *in-situ* HT-XRD. Fig. 1(a–b) show the X-ray diffraction patterns at selected temperatures in the heating and cooling process, respectively. The upper inserts show the two main peaks of BFO as index of (104) and (110). During the heating process, BFO keeps rhombohedral *R3c* structure and no phase transition occurs. The shift of 2θ-values towards smaller Bragg angles is observed in the XRD patterns, which means that heating could make the lattice parameters transition, indicating the thermal expansion behavior. However, the main peak of $Bi_{25}FeO_{39}$ as index of (201) is observed during the cooling process from 700 ℃ to 25 ℃ as shown in the upper left insert in Fig. 1(b), which demonstrates the decomposition of metastable $BiFeO_3$.

BSE images and EDS quantitative analysis results of the sample before and after HT-XRD analyzing are shown in Fig. 2. It is clearly seen that some white phases (Bi-rich $Bi_{25}FeO_{39}$ and Fe-rich $Bi_2Fe_4O_9$) are dispersed on the boundary of gray phases ($BiFeO_3$). The decomposition equation of $BiFeO_3$ will be[13,15]:

$$49BiFeO_3 \rightarrow Bi_{25}FeO_{39} + 12Bi_2Fe_4O_9 \qquad (1)$$

This decomposition suggests that $BiFeO_3$ shows thermodynamic instability behavior in the cooling process, which is different from that in the heating process. The decomposition reaction could be assimilated to a first-order transition, and the nucleation is required[20]. In addition, the shift of 2θ-values towards bigger Bragg angles in the cooling process could indicate the negative thermal expansion behavior. To further study the detailed changes of the lattice constants transition, Rietveld refinements are performed using TOPAS software.

Fig. 3 shows the typical measured and simulated XRD patterns of BFO samples before and after heating process (room temperature, 25 ℃). BFO and a little amount of $Bi_{25}FeO_{39}$ phase (weight percentage 3.5%) were refined with *R3c* and *I23* structural model, respectively. All the criteria R-factors (R_{WP}) are less than 6.5%, which suggests that the refinements are successfully performed. The refined structural parameters in the heating process are summarized in Table 1 and Table 2.

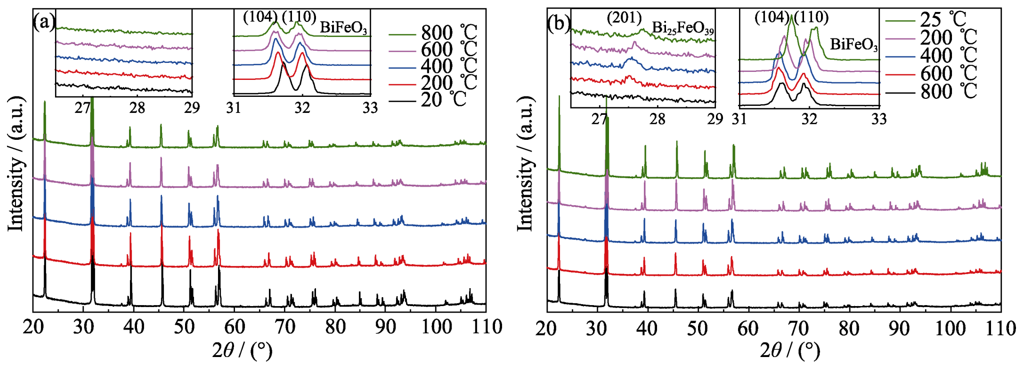

Fig. 1 High temperature XRD patterns of BFO at selected temperatures in the heating (a) and cooling (b) process
Two main peaks of BFO as index of (104) and (110) are shown in upper insert at 31° to 33°;
The main peak of $Bi_{25}FeO_{39}$ as index of (201) is shown in the upper left insert (b)

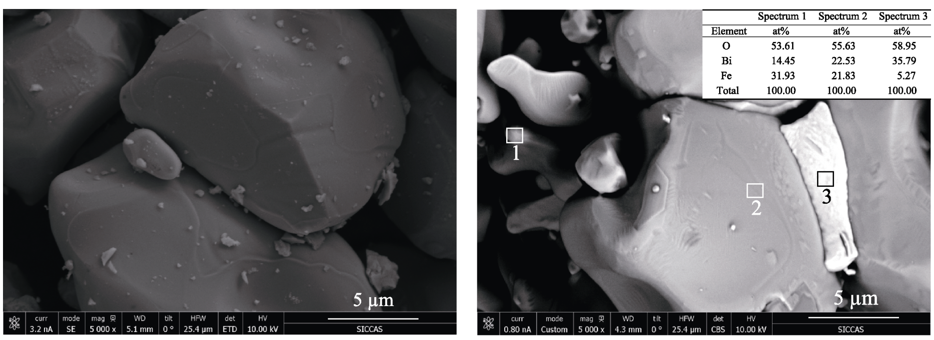

Fig. 2 BSE images and EDS results on the surface of BFO powder before (left) and after (right) heating

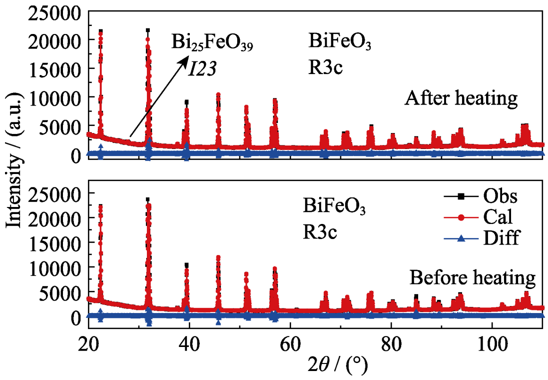

Fig. 3 Observed (black solid lines), calculated (red solid lines) and difference (blue solid lines) XRD patterns of BFO powder before and after heating process

Table 1 Refined lattice parameters of BFO powder in the heating process

T/℃	Lattice parameter		
	a/nm	c/nm	V/nm^3
25	0.5579253(74)	1.387086(20)	0.373926(11)
100	0.5582803(68)	1.388433(20)	0.374766(11)
200	0.5588673(71)	1.390434(20)	0.376096(11)
300	0.5594514(79)	1.392472(23)	0.377435(12)
400	0.5601610(83)	1.394704(24)	0.378999(13)
500	0.5608080(19)	1.396426(49)	0.380344(29)
600	0.5614370(21)	1.397813(54)	0.381577(32)
700	0.5621000(24)	1.398977(61)	0.382797(36)
800	0.5628300(22)	1.399778(58)	0.384011(34)

Table 2 Refined structural parameters of BFO powder in the heating process

T/℃	Atom position									R_{wp}/%
	Bi			Fe			O			
	x	y	z	x	y	z	x	y	z	
25	0	0	0	0	0	0.22124(27)	0.46400(22)	0.01990(16)	0.95452(57)	5.87
100	0	0	0	0	0	0.22129(30)	0.46160(21)	0.02330(17)	0.95583(57)	5.98
200	0	0	0	0	0	0.22227(29)	0.44790(19)	0.02350(18)	0.95600(65)	6.05
300	0	0	0	0	0	0.22039(28)	0.45230(18)	0.03560(17)	0.95718(64)	5.96
400	0	0	0	0	0	0.22192(29)	0.43660(18)	0.02550(18)	0.95829(68)	5.82
500	0	0	0	0	0	0.22325(32)	0.42590(23)	0.01370(23)	0.95869(84)	5.88
600	0	0	0	0	0	0.22484(36)	0.41590(23)	0.01790(24)	0.96229(85)	6.07
700	0	0	0	0	0	0.22400(38)	0.43700(19)	0.00720(18)	0.95701(67)	5.6
800	0	0	0	0	0	0.22376(49)	0.43290(20)	0.01880(21)	0.95832(77)	6.02

The temperature dependences of lattice parameters (a, c) and unit-cell volumes (V) for BFO in the heating and cooling process are shown in Fig. 4. The variation of the lattice parameters (a, c) and unit-cell volumes (V) with temperature could be fitted to a linear function[21-22]. It can be observed that the lattice parameters and unit-cell volumes of BFO increase and decrease monotonically in the heating or cooling process, respectively. This linear fitting also suggests that no structural phase transition occurred for BFO.

Fig. 5 shows the relative changes of lattice parameters and cell volumes for BFO in the heating process. The black, blue and red dash lines represent the values calculated from the linear fit of the lattice parameters and cell volumes. The thermal linear and volumetric expansion coefficients of BFO in the heating process (25–800 ℃)

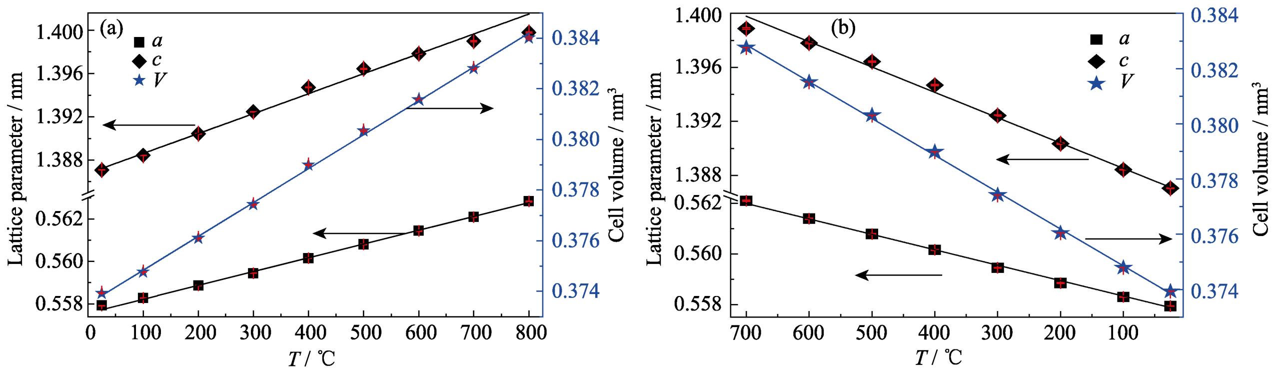

Fig. 4 Lattice parameters and cell volume of BFO in the heating process (temperature regime 25–800 ℃, (a)) and cooling process (temperature regime 700–25 ℃, (b))

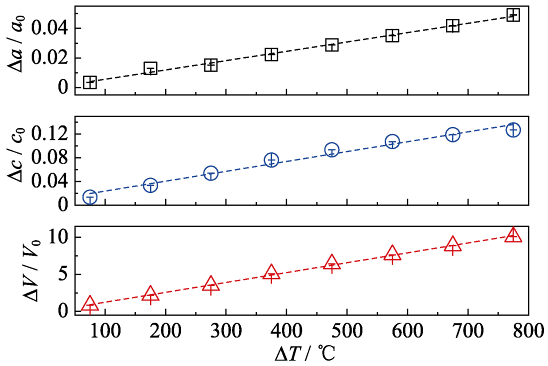

Fig. 5　Relative changes in lattice parameters of BFO as a function of temperature in the heating process

are calculated with the following equation[20-21,23]:

$$\alpha_T^x = \frac{x - x_0}{x_0(T - T_0)} = \frac{\Delta x}{x_0 \Delta T} \quad (2)$$

Where x denotes a, c, and V at selected high temperatures, and x_0 denotes the value of a, c, and V at 25 ℃. The calculated thermal linear and volumetric expansion coefficients of BFO are listed in Table 3, which show an isotropic and positive behavior. It was suggested that the rhombohedral structure with the space group of $R3c$ is very stable, which could be the possible mechanism for their non-phase transition and lower thermal expansion behavior during the heating process.

To establish qualitatively the temperature dependent structural evolution, we further analyze the bond length/bond angle. The atomic positional and occupancy parameters of BFO in the heating process are calculated and refined by the least squares method using TOPAS software. The chemical bonding behavior are determined from this Rietveld refinement. For the G-type structure with space group $R3c$ of $BiFeO_3$, the tilting of FeO_6 octahedron represents the rhombohedral distortion of the perovskite structure. Fig. 6 exhibits the two types of Fe–O bond lengths and the inter-octahedral O–Fe–O angles in the heating process[24]. Fe–O (I) and Fe–O (II) bond lengths basically maintain invariable and slowly increase in the temperature range of 25–400 ℃, respectively. However, Fe–O (I) bond lengths dramatically increase above 400 ℃, Fe–O (II) bond length drops suddenly around 700 ℃. In addition, We note, the O–Fe–O bond angles exhibit compression in the temperature range of 300–600 ℃. After that, these bond angles show

Table 3　The thermal linear and volumetric expansion coefficients of pure BFO

Sample	Temperature/℃	α_T^a/ $(\times10^{-6}, ℃^{-1})$	α_T^c/ $(\times10^{-6}, ℃^{-1})$	α_T^V/ $(\times10^{-6}, ℃^{-1})$
$BiFeO_3$	25–800	11.34	11.81	34.80

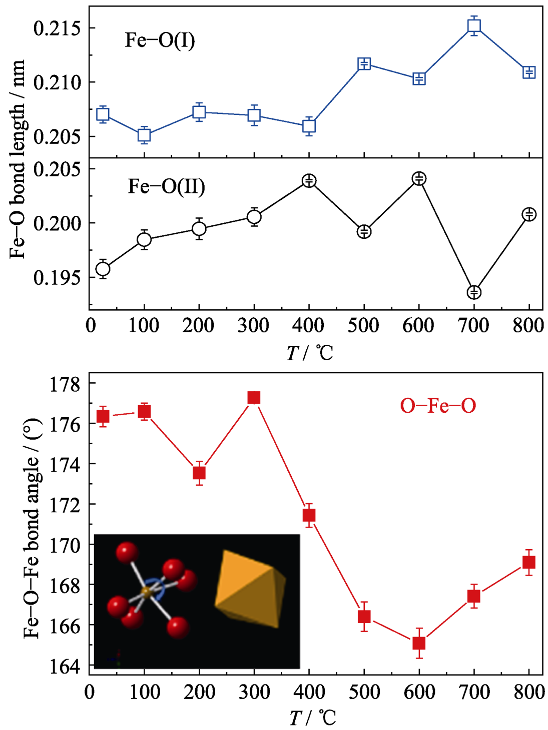

Fig. 6　Fe–O bond lengths and Fe–O–Fe angles of BFO in the heating process

an increase upon heating above 600 ℃, which consequently induces tilts oxygen octahedron and expansion of the unit cell[25]. This oxygen octahedron tilt distortion may result in the decomposition of $BiFeO_3$.

Fig. 7 shows the Raman spectra of BFO at selected temperatures in the heating process. For BFO at 25 ℃, three strong peaks at 138, 172, 219 cm^{-1} and one weak peak around 427 cm^{-1} are assigned as A_1-1, A_1-2, A_1-3 and A_1-4 mode, respectively. The peaks at 259, 283, 321, 349, 475, 523, and 553 cm^{-1} belong to E mode[26]. In the heating process, BFO keeps its structure which is in agreement with the HT-XRD results. Increasing temperature results in the shift (toward lower wavenumber) and broaden of Raman bands, which is explained in terms of thermal expansion and oxygen octahedron tilt distortion.

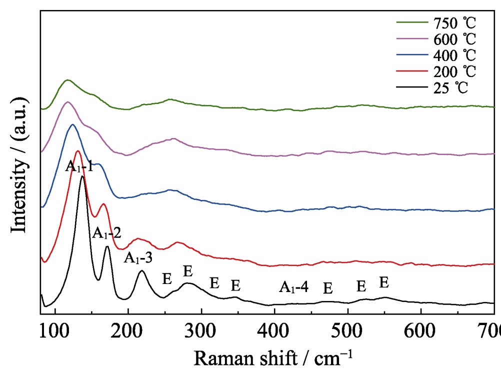

Fig. 7　Raman spectra of BFO at selected temperatures in the heating process

3 Conclusion

In this study, the thermodynamic stability, decomposition and thermal expansion of pure $BiFeO_3$ are studied systematically. BFO keeps its rhombohedral structure with the space group of *R3c*. The temperature dependences of the relative lattice parameters and cell volume for the BFO are linear, suggesting that, in the heating process (25–800 ℃), no structural phase transition occurs. However, minor $BiFeO_3$ could decompose to $Bi_2Fe_4O_9$ and $Bi_{25}FeO_{39}$ in the cooling process. The oxygen octahedron tilt distortion reflected by the change in bond length may result in the decomposition of $BiFeO_3$. The thermal linear and volumetric expansion coefficients of BFO in the heating process are calculated, which show an isotropic and positive behavior.

References:

[1] CARVALHO T T, TAVARES P B. Synthesis and thermodynamic stability of multiferroic $BiFeO_3$. *Mater. Lett.*, 2008, **62(24):** 3984–3986.
[2] BERNARDO M S, JARDIEL T, PEITEADO M, *et al.* Reaction pathways in the solid state synthesis of multiferroic $BiFeO_3$. *J. Eur. Ceram. Soc.*, 2011, **31(16):** 3047–3053.
[3] RANGI M, SANGHI S, JANGRA S, *et al.* Crystal structure transformation and improved dielectric and magnetic properties of La-substituted $BiFeO_3$ multiferroics. *Ceram. Int.*, 2017, **43(15):** 12095–12101.
[4] MICHEL C, MOREAU J M, ACHENBACH G D, *et al.* The atomic structure of $BiFeO_3$. *Solid State Com.*, 1969, **7(9):** 701–704.
[5] CHATURVEDI S, BAG R, SATHE V, *et al.* Holmium induced enhanced functionality at room temperature and structural phase transition at high temperature in bismuth ferrite nanoparticles. *J. Mater. Chem. C*, 2016, **4(4):** 780–792.
[6] WEI J, HAUMONT R, JARRIER R, *et al.* Nonmagnetic Fe-site doping of $BiFeO_3$ multiferroic ceramics. *Appl. Phys. Lett.*, 2010, **96(10):** 102509.
[7] GAUTAM A, RANGRA V S. Effect of Ba ions substitution on multiferroic properties of $BiFeO_3$ perovskite. *Cryst. Res. Technol.*, 2010, **45(9):** 953–956.
[8] NALWA K S, GARG A, UPADHYAYA A. Effect of samarium doping on the properties of solid-state synthesized multiferroic bismuth ferrite. *Mater. Lett.*, 2008, **62(6/7):** 878–881.
[9] WANG Y P, ZHOU L, ZHANG M F, *et al.* Room-temperature saturated ferroelectric polarization in $BiFeO_3$ ceramics synthesized by rapid liquid phase sintering. *Appl. Phys. Lett.*, 2004, **84(10):** 1731–1733.
[10] ZHANG S T, LU M H, WU D, *et al.* Larger polarization and weak ferromagnetism in quenched $BiFeO_3$ ceramics with a distorted rhombohedral crystal structure. *App. Phy. Lett.*, 2005, **87(26):** 262907.
[11] SELBACH S M, TYBELL T, EINARSRUD M A, *et al.* Size-dependent properties of multiferroic $BiFeO_3$ nanoparticles. *Chem. Mater.*, 2007, **19:** 6478–6484.
[12] ZHANG L, CAO X F, MA Y L, *et al.* Polymer-directed synthesis and magnetic property of nanoparticles-assembled $BiFeO_3$ microrods. *J. Solid. State. Chem.*, 2010, **183(8):** 1761–1766.
[13] KUMAR M M, PALKAR V R, SRINIVAS K, *et al.* Ferroelectricity in a pure $BiFeO_3$ ceramic. *Appl. Phys. Lett.*, 2000, **76(19):** 2764–2766.
[14] SELBACH S M, EINARSRUD M A, GRANDE T. On the thermodynamic stability of $BiFeO_3$. *Chem. Mater.*, 2009, **21(1):** 169–173.
[15] CHENG G F, RUAN Y J, LIU W, *et al.* Effect of temperature variation on the phase transformation in the reaction sintering of $BiFeO_3$ ceramics. *Mater. Lett.*, 2015, **143:** 330–332.
[16] CHEN J, FAN L, REN Y, *et al*, Unusual transformation from strong negative to positive thermal expansion in $PbTiO_3$-$BiFeO_3$ perovskite. *Phys. Rev. Lett.*, 2013, **110:** 115901.
[17] BHATTACHARJEE S, TAJI K, MORIYOSHI C, *et al.* Temperature-induced isostructural phase transition, associated large negative volume expansion, and the existence of a critical point in the phase diagram of the multiferroic (1-x)$BiFeO_3$-$x$$PbTiO_3$ solid solution system. *Phys. Rev. B*, 2011, **84(10):** 104116.
[18] KLYNDYUK A I, CHIZHOVA E A. Structure, thermal expansion, and electrical properties of $BiFeO_3$-$NdMnO_3$, solid solutions. *Inorg. Mater.*, 2015, **51(3):** 272–277.
[19] CHEN J, XING X R, LIU G R. Structure and negative thermal expansion in the $PbTiO_3$-$BiFeO_3$ system. *Appl. Phys. Lett.*, 2006, **89:** 101914.
[20] PALAI R, KATIYAR R S, SCHMID H, *et al.* β, phase and γ-β, metal-insulator transition in multiferroic $BiFeO_3$. *Phys. Rev. B*, 2008, **77(1):** 014110.
[21] GUSEV A I, SADOVNIKOV S I, CHUKIN A V, *et al.* Thermal expansion of nanocrystalline and coarse-crystalline silver sulfide Ag_2S. *Phys. Solid State*, 2016, **58(2):** 251–257.
[22] KESKAR M, KRISHNAN K, DAHALE N D. Thermal expansion studies on $Th(MoO_4)_2$, $Na_2Th(MoO_4)_3$, and $Na_4Th(MoO_4)_4$. *J. Alloys Compounds*, 2008, **458(1):** 104–108.
[23] HALVARSSON M, LANGER V, VUORINEN S. Determination of the thermal expansion of κ-Al_2O_3, by high temperature XRD. *Surf. Coat. Tech.*, 1995, **76-77(5):** 358–362.
[24] KUBEL F, SCHMID H. Structure of a ferroelectric and ferroelastic monodomain crystal of the perovskite $BiFeO_3$. *Acta Cryst.*, 1990, **B46:** 698–702.
[25] FIZA M, HASSNAIN J G, ISMAT S S. Peculiar magnetism in Eu substituted $BiFeO_3$ and its correlation with local structure. *J. Phys.:Condens. Matter*, 2018, **30:** 435802.
[26] PANDEY R, PANDA C, KUMAR P, *et al.* Phase diagram of Sm and Mn co-doped bismuth ferrite based on crystal structure and magnetic properties. *J. Sol-Gel Sci. Technol.*, 2018, **85:** 166–177.

纯相 $BiFeO_3$ 的热稳定和热膨胀性质研究

程国峰，阮音捷，孙 玥，尹晗迪

(中国科学院 上海硅酸盐研究所，无机材料分析测试中心，上海 200050)

摘 要: 本研究利用原位高温衍射和高温拉曼技术对纯相 $BiFeO_3$ 粉体的热稳性和热膨胀性质进行了系统的解析。在升温阶段 $BiFeO_3$ 始终保持斜方的 *R3c* 结构，但是在降温阶段少量 $BiFeO_3$ 会分解成为 $Bi_2Fe_4O_9$ 和 $Bi_{25}FeO_{39}$，这种分解可能是由氧八面体的倾斜畸变引起的。此外，还研究了 $BiFeO_3$ 热力学膨胀系数，发现它具有各向同性正膨胀性。以上结果也被拉曼光谱所证实。本研究的结果可为制备纯相 $BiFeO_3$ 材料提供实验指导。

关 键 词: 铁酸铋；相变；热膨胀系数；高温 X 射线衍射；高温拉曼光谱

中图分类号: TQ174 **文献标识码:** A